High Velocity Oxy-Fuel (HVOF) Suspension Spraying of Mullite Coatings

Oberste Berghaus, J.; Marple, B. R.l

Publisher's version / la version de l'éditeur:
Journal of Thermal Spray Technology, 17, 5-6, pp. 671-678, 2008

Web page / page Web
http://dx.doi.org/10.1007/s11666-008-9219-8
http://nparc.cisti-icist.nrc-cnrc.gc.ca/npsi/ctrl?action=rtdoc&an=11344015&lang=en
http://nparc.cisti-icist.nrc-cnrc.gc.ca/npsi/ctrl?action=rtdoc&an=11344015&lang=fr

JTTEE5 17:671–678
DOI: 10.1007/s11666-008-9219-8
1059-9630/$19.00 © ASM International

High-Velocity Oxy-Fuel (HVOF) Suspension Spraying of Mullite Coatings

J. Oberste Berghaus and B.R. Marple

(Submitted May 1, 2008)

Mullite coatings ($3Al_2O_3 \cdot 2SiO_2$) were deposited by suspension thermal spraying of micron-sized ($D_{50} = 1.8$ μm) feedstock powders, using a high-velocity oxy-fuel gun (HVOF) operated on propylene (DJ-2700) and hydrogen fuels (DJ-2600). The liquid carrier employed in this approach allows for controlled injection of much finer particles than in conventional thermal spraying, leading to coatings with low porosity and fine and homogeneous porosity distribution, making this process potentially suitable for creating thin layers with low gas permeability. In-flight particle states were measured for a number of spray conditions of varying fuel-to-oxygen ratios and standoff distances and related to the resulting microstructure, stoichiometry, phase composition (EDS, SEM, XRD), and hardness (VHN_{300gf}) of the coatings. In an attempt to retain the crystalline phase in the coatings, HVOF operating conditions were varied to limit in-flight particle melting. However, fully crystalline coatings were only obtained by gradually heating the coating during deposition to temperatures above 400 °C.

Keywords HVOF suspension spraying, mullite coatings, suspension thermal spraying

1. Introduction

Mullite, an aluminosilicate of composition $3Al_2O_3 \cdot 2SiO_2$, has attracted considerable interest as a protective coating in high-temperature applications due to its high thermal and chemical stability, low thermal expansion coefficient, low thermal conductivity, and low oxygen permeability, associated with the sealing properties of silica. Over the entire temperature range of the crystalline phase, no polymorphic phase transitions occur, which results in particularly high thermal shock resistance and high strength (Ref 1-3). Mullite-based protective and thermal barrier coatings are applied in heat exchangers, gas turbines, and internal combustion engines, i.e., diesel engines, often in combination with SiC or Si_3N_4 thermal barriers by virtue of similar thermal expansion coefficients and chemical compatibility (Ref 4, 5). In particular, mullite coatings are often used in environmental barrier coating (EBC) systems as a basic protection against oxidative or water vapor-containing atmospheres at elevated temperatures (Ref 6, 7).

Plasma sprayed mullite is generally reported to contain a high portion of amorphous phase due to the rapid solidification of the molten droplets during the coating formation. Recrystallization during service at 700-1000 °C has been reported to cause cracking and delamination from the substrate due to the associated volume reduction of about 0.4% (Ref 1) By heating the substrate above the crystallization temperature (>980°) inside a furnace during spraying, desired crystallinity can be created directly in the spray process (Ref 4). This method is well suited for SiC substrates, but has limited use for metallic substrates, being subject to high-temperature oxidation. Other efforts are directed toward carefully limiting the thermal energy delivered to relatively large (>44 μm) crystalline feedstock powders by adjusting the thermal spray conditions, thereby fostering only partial melting of the particles and retaining above 80% of the original crystallinity in the coating (Ref 8, 9). Due to a low remaining amorphous content, the resulting recrystallization stresses are reported to be of less concern. To overcome some disadvantages inherently associated with the use of large feedstock particles for protective coatings, such as large coating thickness, coarse porosity, and high surface roughness, Siegert et al. (Ref 10) reports the use of a sol-gel feedstock with mullite precursors in a plasma spray process. The desired coating crystallinity and low porosity is attained by repeatedly passing over the layer with the plasma flame after deposition, thereby effectively reheating and in situ recrystallizing the coating. Similarly, the amorphous phase formation can somewhat be avoided in conventional thermal sprayed mullite coatings by hot spraying, i.e., maintaining high substrate temperature conditions during deposition, as illustrated by Vassen et al.

This article is an invited paper selected from presentations at the 2008 International Thermal Spray Conference and has been expanded from the original presentation. It is simultaneously published in *Thermal Spray Crossing Borders, Proceedings of the 2008 International Thermal Spray Conference*, Maastricht, The Netherlands, June 2-4, 2008, Basil R. Marple, Margaret M. Hyland, Yuk-Chiu Lau, Chang-Jiu Li, Rogerio S. Lima, and Ghislain Montavon, Ed., ASM International, Materials Park, OH, 2008.

J. Oberste Berghaus and **B.R. Marple**, Industrial Materials Institute, NRC, 75 de Mortagne Blvd., Boucherville, QC, Canada J4B 6Y4. Contact e-mail: jorg.oberste-berghaus@bekaert.com.

(Ref 6) for mullite coatings on siliconized carbon reinforced carbon substrates.

High-velocity oxy-fuel (HVOF) suspension spraying is an emerging technology that permits better feeding and spraying of finer particles than conventional thermal spraying (Ref 11, 12). In principle, thinner coatings (20-100 μm) with more refined microstructures and potentially smoother surface finishes are created. Feeding micron-sized or submicron particles into a thermal spray gun with conventional equipment is virtually impossible due to the strong powder agglomeration, which impedes dry powder flow. Suspending the small particles in a liquid carrier, which is then injected into the HVOF gun, alleviates this problem and allows for precisely controlled feeding rates. In the HVOF combustion chamber, the suspension is atomized into a fine mist and the suspension medium is evaporated and combusted along with the fuel, thereby concentrating the solid content into micro-sized particles, which are then projected toward a substrate. The high particle velocity of HVOF systems is conducive for creating dense, and possibly gas impermeable, coatings. Furthermore, the maximum flame temperature in HVOF is substantially lower (2500-3100 °C) than in plasma systems (>8000 °C), which may, in the case of small mullite particles, limit complete particle melting to retain some of the original crystallinity. The lower flame temperature may also be advantageous in avoiding segregation into silica- and alumina-rich phases and consequent silica evaporation and loss.

In this study, the potential of this technique for creating thin, dense, and finely structured mullite coatings with some remaining crystallinity is explored. The suspension feedstock is axially injected into the combustion chamber of an HVOF gun. In-flight particle velocity and temperature are measured for different operating conditions and standoff distances, and related to the resulting microstructure and phase composition of the coating. Different HVOF fuels, i.e., propylene and hydrogen, and different fuel-to-oxygen ratios are compared. Finally, in situ recrystallization by gradually heating the coating to high temperatures during deposition is investigated.

2. Experimental

Suspension spraying was implemented using an HVOF DJ-2700 (propylene-C_3H_6) and DJ-2600 (hydrogen-H_2) hybrid gun (Sulzer-Metco, Westbury, NY). The systems were equipped with internal injection/atomization modules inserted into the standard powder feeding ports, thereby intimately contacting the coaxially fed suspension droplets with the fuel inside the HVOF combustion chamber. The suspensions were delivered by a prototype Nanofeed Liquid Powder Feeder (Model 640, Northwest Mettech, North Vancouver, Canada). Flow-rate control, start-up, shutdown, and rinsing sequences were fully automated and PC controlled. The injection module and fuel distributor were continuously cooled with nitrogen at a flow rate of 15 slpm, also serving as atomizing gas.

Table 1 DJ-2700 and DJ-2600 HVOF spray parameters

Parameter	Value
Propylene flow (DJ-2700)	85, 75, 65, 55 and 50 slpm
Oxygen flow (DJ-2700)	279 slpm
Air flow (DJ-2700)	202 slpm
Hydrogen flow (DJ-2600)	684 and 450 slpm
Oxygen flow (DJ-2600)	231 slpm
Air flow (DJ-2600)	330 slpm
Carrier gas (N_2) flow	15 slpm
Suspension feed rate	50 mL/min (3.0 kg/h)
Spray distance	7.6-12.7 cm
Gun traverse speed	762 mm/s

In addition, coolant medium, such as nitrogen, water, or suspension, was delivered through the feeding port at all times during operation of the gun to prevent overheating and possible blockage of the internal components. The system was adapted to deliver the suspension feed against the combustion backpressure of up to 6.46 atm in the case of propylene and up to 7.48 atm for hydrogen. In an attempt to vary particle temperature at high velocities, the gun was operated with the two different fuels of varying flow rates, while maintaining constant air and oxygen flows, respectively, as summarized in Table 1.

In-flight particle states were measured with a commercial diagnostic system (AccuraSpray® G2 Tecnar, St-Bruno, PQ, Canada). The temperature measurement is based on two-color pyrometry, and the velocity is determined by a time-of-flight technique. At a short spray distance of 7.6 cm from the gun nozzle exit, measurements of particle temperature and velocity were impeded by the presence of compression/decompression zones (shock barrels) in the supersonic flame. Based on measurements further downstream at 7.6-15.2 cm from the nozzle, an indirect approach to rank the in-flight particle states for each set of spray parameters was adopted.

Microstructures of the coatings were observed by SEM (JEOL JSM-610) and FE-SEM (Hitachi S4700). The samples were prepared by standard metallographic methods. Porosity was assessed on the cross section by SEM (1000 X), using image analysis. Such magnification was judged most suitable to capture the finely structured porosity in the coatings. The intensity range and thresholds were standardized on reference materials and ten measurements were averaged per sample. Elemental composition was measured by energy dispersive spectroscopy (EDX) at 500X magnification, averaging three measurements per sample.

Vickers microhardness measurements were performed under a 300 g load for 20 sec on the polished cross section of the coatings and ten measurements were averaged per sample.

Phase analysis was carried out by XRD using a Brucker D8-Discovery diffractometer (Brucker AXS Inc. Madison) with Cu-K_α radiation at an acquisition of 0.01°/sec. In an attempt to compare the degree of crystallinity between the coatings, the ratio of peak areas between 20 and 50° to the total integrated area in this region, including the diffuse amorphous hump, was measured and denoted here as index of crystallinity (IC). Particle sizes and distribution

were measured with a Coulter LS Particle size analyzer (Beckman Coulter Canada Inc., Mississauga, Canada) using a liquid module.

Fused and crushed feedstock powders of high-purity mullite (Chichibu MP40, Scimarec Co. Ltd., Tokyo, Japan) with a nominal particle size of 1-2 μm were used in this study. Powder morphology is shown in Fig. 1.

Suspensions were prepared with 5wt.% solids in a mixture of ethanol and 30wt.% ethylene glycol. Polyethylenimine (MWT 25,000 Alfa Aesar) was used as dispersing agent. The pH of the suspension was adjusted to neutral conditions using nitric acid. The addition of viscous ethylene glycol further prolonged the settling time of the suspension. The procedure stabilized the dispersion sufficiently to be compatible with the spray process.

The size distribution of the particles and agglomerates in suspension is shown in Fig. 2. The powder shows a relatively narrow size distribution with D_{50} = 1.8 μm, but submicron satellite particles as well as aggregates as large as 10 μm are also present.

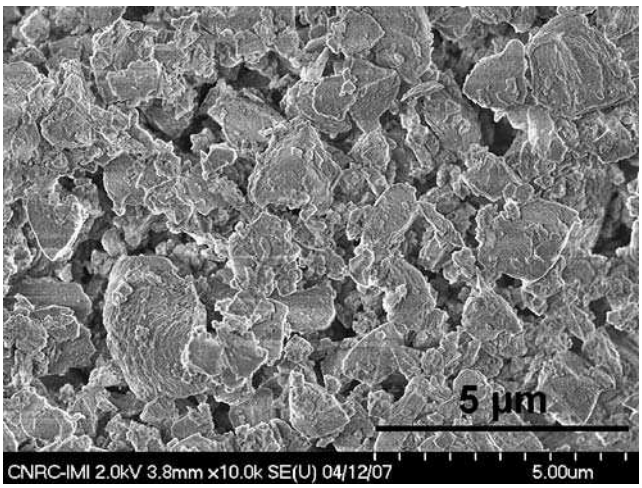

Fig. 1 Micrograph of MP40 mullite feedstock

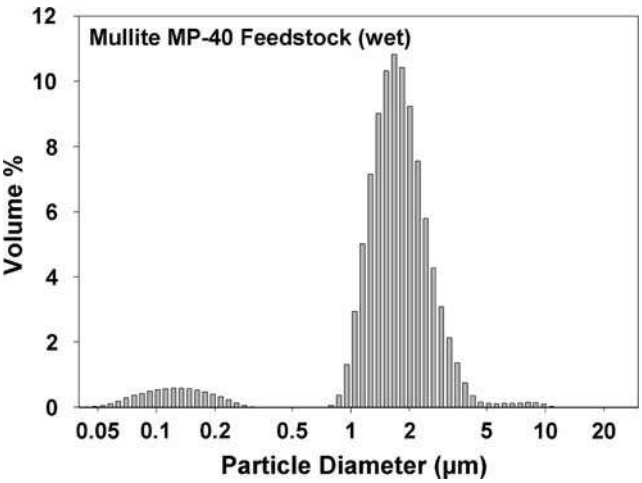

Fig. 2 Particle size distribution in feed suspension

Coatings were produced on mild steel substrates with dimensions of 25 × 75 × 12.5 mm. To increase coating adhesion, the substrate surface was grit-blasted with 54 grit Al_2O_3 particles prior to deposition. For most coatings, the surface temperature, as monitored with a pyrometer, was maintained at 250-300 °C during deposition by using forced air cooling. The substrate was preheated to approximately 200 °C by the HVOF flame in 10 passes immediately before deposition. Selected coatings were produced at an elevated surface temperature of up to 420 °C.

3. Results and Discussion

3.1 DJ-2700 Coatings

A typical microstructure of the coatings produced at a standard condition with propylene fuel (85 slpm) at a spray distance of 7.6 cm is shown in Fig. 3. Depending on the exact operating conditions, deposition rates varied from 6.3 to 7.5 um/pass. Deposition efficiencies were measured between 50 and 65% at spray distances up to

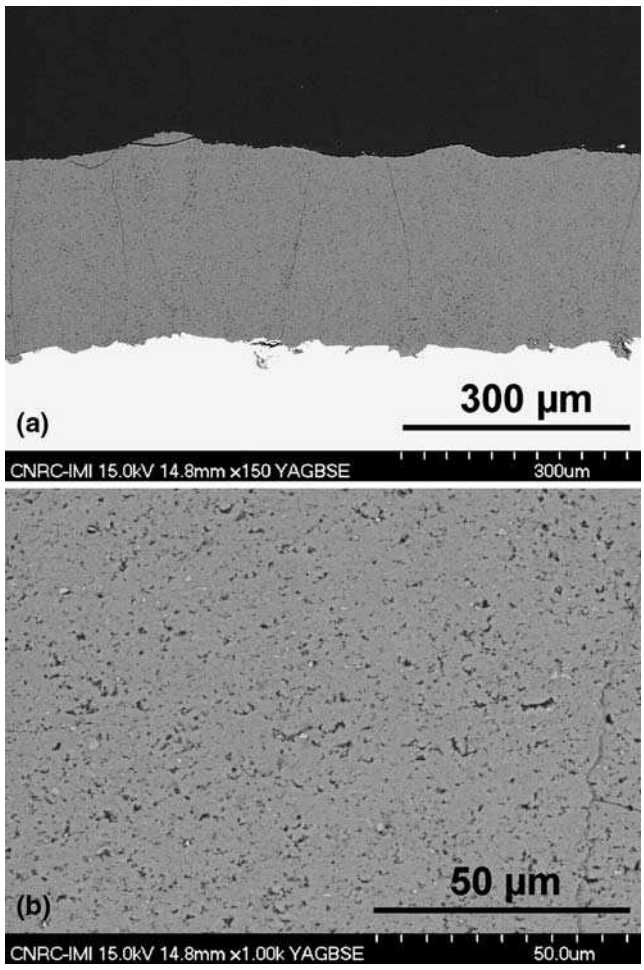

Fig. 3 Micrographs of cross sections of DJ-2700 coating (85 slpm C_3H_6 at SD 7.6 cm)

12.6 cm. Typical coating thicknesses were between 110 and 130 μm. Coatings up to 260 μm in thickness were also produced. The initial layers of the coating filled the original surface features of the grit-blasted substrate, resulting in a final surface roughness of $R_a < 3.5$ μm, as measured with a profilometer.

The porosity of the sample shown in Fig. 3 is 1.4 ± 0.4%, but varied between 0.9% and 3.4% for coatings produced at the shortest spray distance (7.6 cm), depending on the exact fuel and gun conditions. The elemental composition of the DJ-2700 coatings (85 slpm C_3H_6) is summarized in Table 2. Besides a slight loss in oxygen, the stoichiometric ratio of Al to Si, corresponding to the mullite feedstock, is preserved in the coatings.

3.2 Spray Distance

In-flight particle states as a function of standoff distance are exemplified in Fig. 4 for this particular spray condition (85 slpm C_3H_6). The large error bars indicate significant uncertainty in the temperature measurement close to the gun nozzle exit. However, the temperature and velocity decrease monotonically from approximately 2500 °C and 850 m/s (at.7.6 cm), imparting some confidence to the measurement.

Coatings were produced at different standoff distances, using the same spray conditions. An increase in SD leads to a rise in porosity of up to 9%, as shown in Fig. 5. Correspondingly, the Vickers indentation hardness decreases from 623 $Hv_{0.3}$ to below 400 $Hv_{0.3}$ for the most porous coating. Figure 6 compares the XRD spectra of these coatings with the MP40 feedstock. The spectra show, besides the crystalline mullite peaks, a distinct hump in the region of 20-50°, indicative of a high amorphous content in the coatings.

An increase in porosity and the associated loss in hardness with lower particle temperature and velocity is somewhat expected. It is, however, less evident to observe the decrease in crystallinity, as suggested by the lowering of the peak heights in Fig. 6. Comparing the phase composition in terms of IC, a decrease from 37% at SD 7.6 cm to 17% at SD 10.2 cm and finally to 14% at SD 12.7cm is noted. It is unlikely that different rates of in situ recrystallization of the mullite coatings occurred in this case, since the maximum substrate temperature was carefully maintained at 230-250 °C for the three coatings. It is possible that the particle residence time in the heating combustion flame pays an important role. At the shortest standoff distance, unmolten particles may still be preserved, which deposit by virtue of the very high jet velocity. At larger spray distance, the particles may have had more time to fully melt and increase the amorphous content in the coating.

Table 2 EDX elemental composition

Sample	SD, cm	O, at.%	Al, at.%	Si, at.%
Feed MP40	...	59.0	30.1	10.8
85-P	7.6	55.8 ± 0.7	32.7 ± 0.5	11.5 ± 0.2
85-P	10.2	56.3 ± 0.6	32.4 ± 0.4	11.2 ± 0.2
85-P	12.7	56.3 ± 0.3	32.3 ± 0.4	11.4 ± 0.2

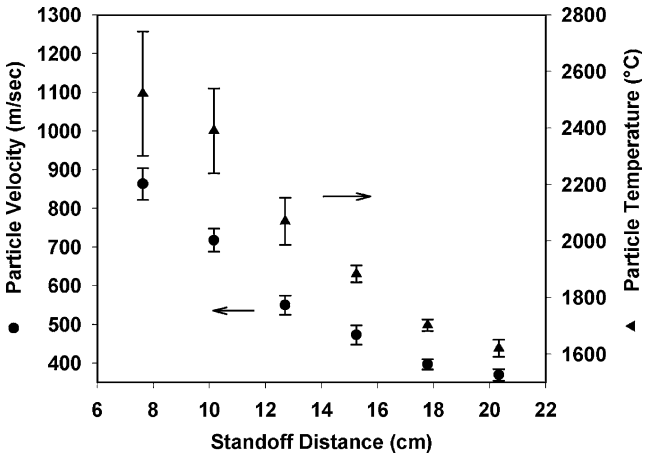

Fig. 4 Particle state versus standoff distance at 85 slpm propylene

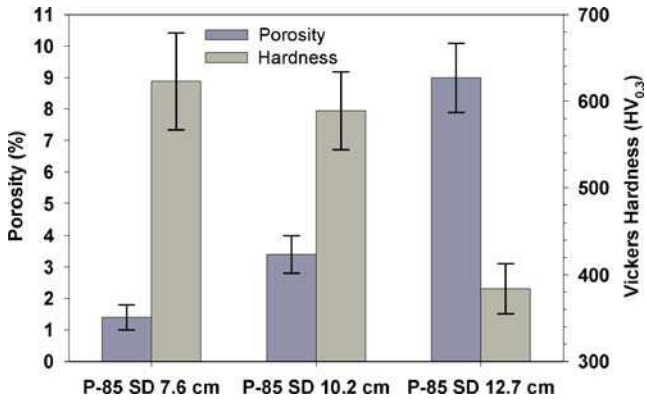

Fig. 5 Porosity and hardness versus standoff distance at 85 slpm propylene condition

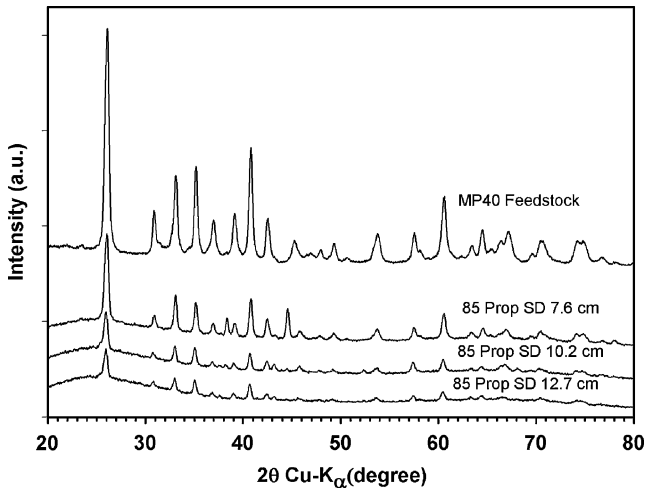

Fig. 6 XRD spectra of MP40 feedstock and coatings produced with 85 slpm propylene fuel

3.3 Fuel-to-Oxygen Ratio

Maximum particle temperatures in HVOF systems depend on, besides the torch design and feed conditions, the fuel-to-oxygen ratio (Ref 11). Figure 7 exemplifies the drop in particle temperature for decreasing propylene fuel rates from 85 to 50 slpm (at constant standoff distance). Replacement of the gun barrel resulted in higher temperature and velocity than reported above. In fact, during the course of the work, a high sensitivity of the coatings and particle states to the conditioning of the gun was noticed.

The characteristics of the corresponding coatings produced at SD of 7.6 cm are summarized in Fig. 8. In spite of the lower particle temperature and velocity with reduced fuel supply, a decrease in coating porosity and crystalline content can be discerned. It is again possible that residence time, and not maximum flame temperature, is a governing factor to limit particle melting to create more porous and crystalline coatings. In this case, high fuel ratios lead to high jet velocity and short dwell times, limiting particle melting, even though the flame temperature is elevated over a condition with less fuel. A trend in coating hardness cannot be identified within the measurement confidence. However, the highest hardness of 646 ± 33 $Hv_{0.3}$ was measured for a coating (Prop-85-hot) produced at much higher substrate temperature, gradually increasing to 410 °C during deposition. A significant densification and in situ crystallization has probably taken place, resulting in a crystalline coating, as measured on its top surface by XRD. The microstructure of this high-temperature coating shows distinct strata formation in its upper portion, composed of layers of spherical pores (Fig. 9a and b). This feature suggests that besides recrystallization, some remelting of the top surface in the last few deposition passes has occurred. A lower surface roughness of R_a 2.7 ± 05 μm, as compared to the coating produced at lower surface temperature (Prop-85) with R_a 3.1 ± 0.7 μm, also supports this idea. The microstructure of this high-temperature coating shows distinct strata formation in its upper portion, composed of layers of spherical pores (Fig. 9a and b). This feature suggests that besides recrystallization, some remelting of the top surface in the last few deposition passes has occurred. A lower surface roughness of R_a 2.7 ± 05 μm, as compared to the coating produced at lower

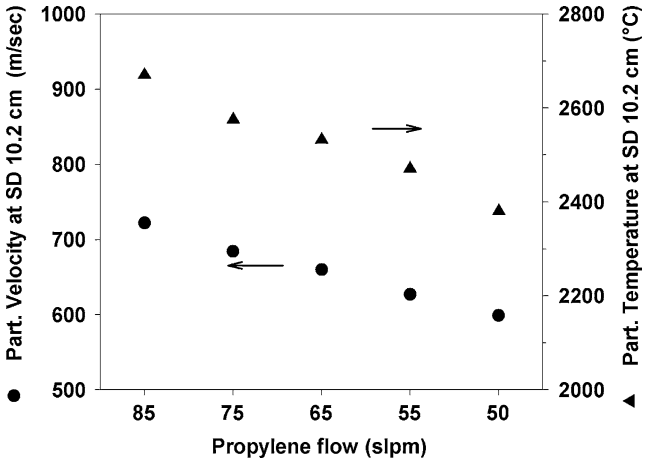

Fig. 7 Particle states for different propylene flows at SD 10.2 cm with new gun barrel

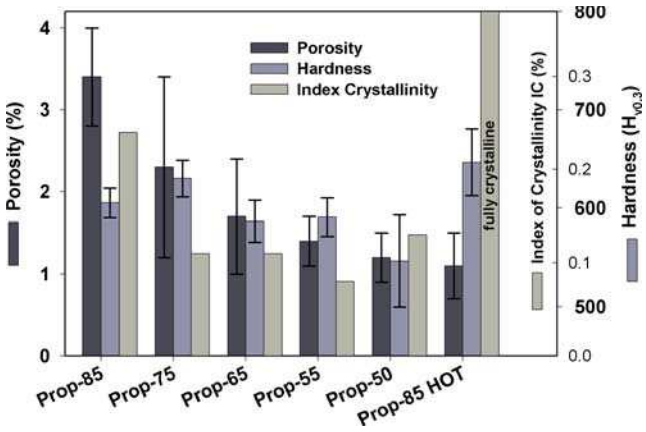

Fig. 8 Coating characteristics versus propylene rate

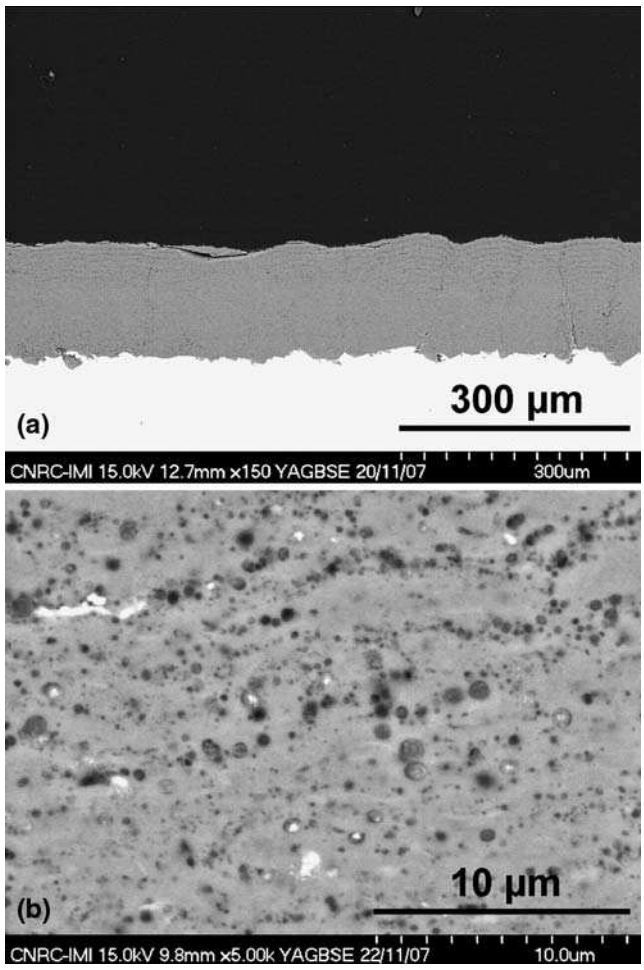

Fig. 9 Microstructure of coating produced at high surface temperature (Prop-85 Hot)

surface temperature (Prop-85) with R_a 3.1 ± 0.7 μm, also supports this idea. It should be noted that within the T-V operating space of the DJ-2700, particle temperature and velocity are strongly coupled and cannot be varied individually, as illustrated in Fig. 10. To retain some coating crystallinity, it was consequently difficult to limit particle melting by both a low flame temperature and a short dwell time at high particle velocity.

3.4 DJ-2600 Coatings

In an attempt to shift the operating space to lower particle temperatures, the system was operated with hydrogen fuel, as illustrated in Fig. 10. Coatings were produced at two different hydrogen flow rates of 684 and 450 slpm, keeping the other operating conditions constant. In this case, reducing the fuel supply from an over-stoichiometric to a close to stoichiometric fuel/oxygen ratio raised both the particle temperature and velocity as measured in Fig. 11.

The characteristics of the coatings produced at the shortest standoff distance (7.6 cm) are summarized in Fig. 12. Comparing samples H_2-684 and H_2-450, the coating becomes slightly denser, harder, and loses some of its remaining crystallinity. In addition, the deposition rate was found to increase from 5.7 to 7.7 μm/pass. Both coatings were produced at a maximum surface temperature of 300 °C.

Again, crystalline coatings, or at least coatings with crystalline top surfaces as measured by XRD, were obtained for both conditions by allowing the substrate temperature to gradually increase to 410 °C during deposition. The XRD spectra of the four coatings are shown in Fig. 13. Representative microstructures of samples produced at cold (H_2-450) and hot substrate temperatures (H_2-684 Hot) are shown in Fig. 14. Similar to the propylene coatings, strata composed of circular pores can be discerned in the top portion of the coating, indicating some surface remelting. It should be mentioned that when a high surface temperature was maintained during the entire deposition time, the coatings were found to spall from the substrate. The above microstructures and characteristics of the DJ-2600 coatings suggest that they

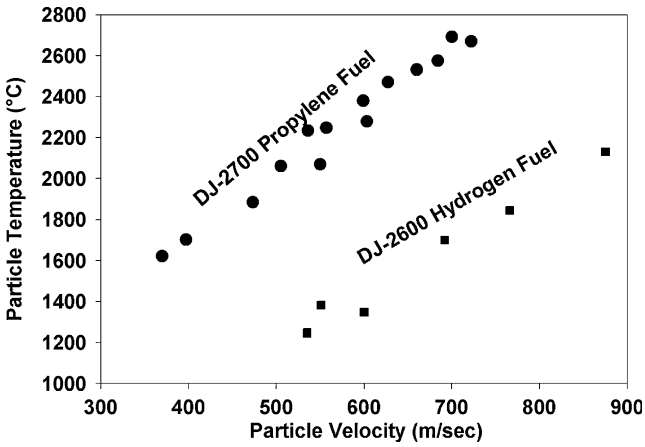

Fig. 10 DJ-2700 and DJ-2600 operating space in terms of particle temperature and velocity

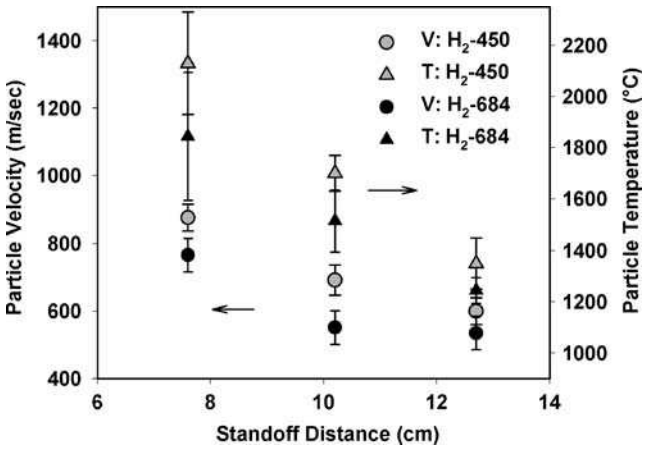

Fig. 11 DJ-2600 particle states versus SD

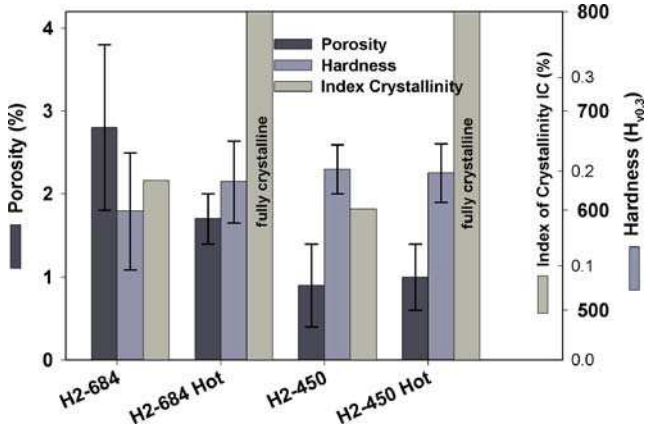

Fig. 12 Coating characteristics versus hydrogen feed rate

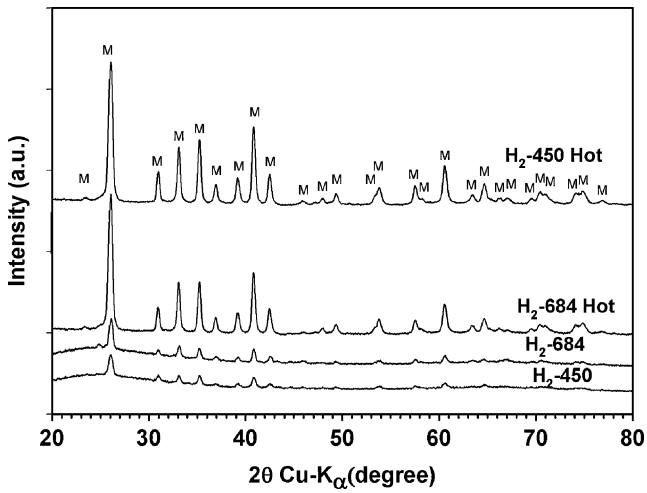

Fig. 13 XRD spectra of DJ-2600 coatings

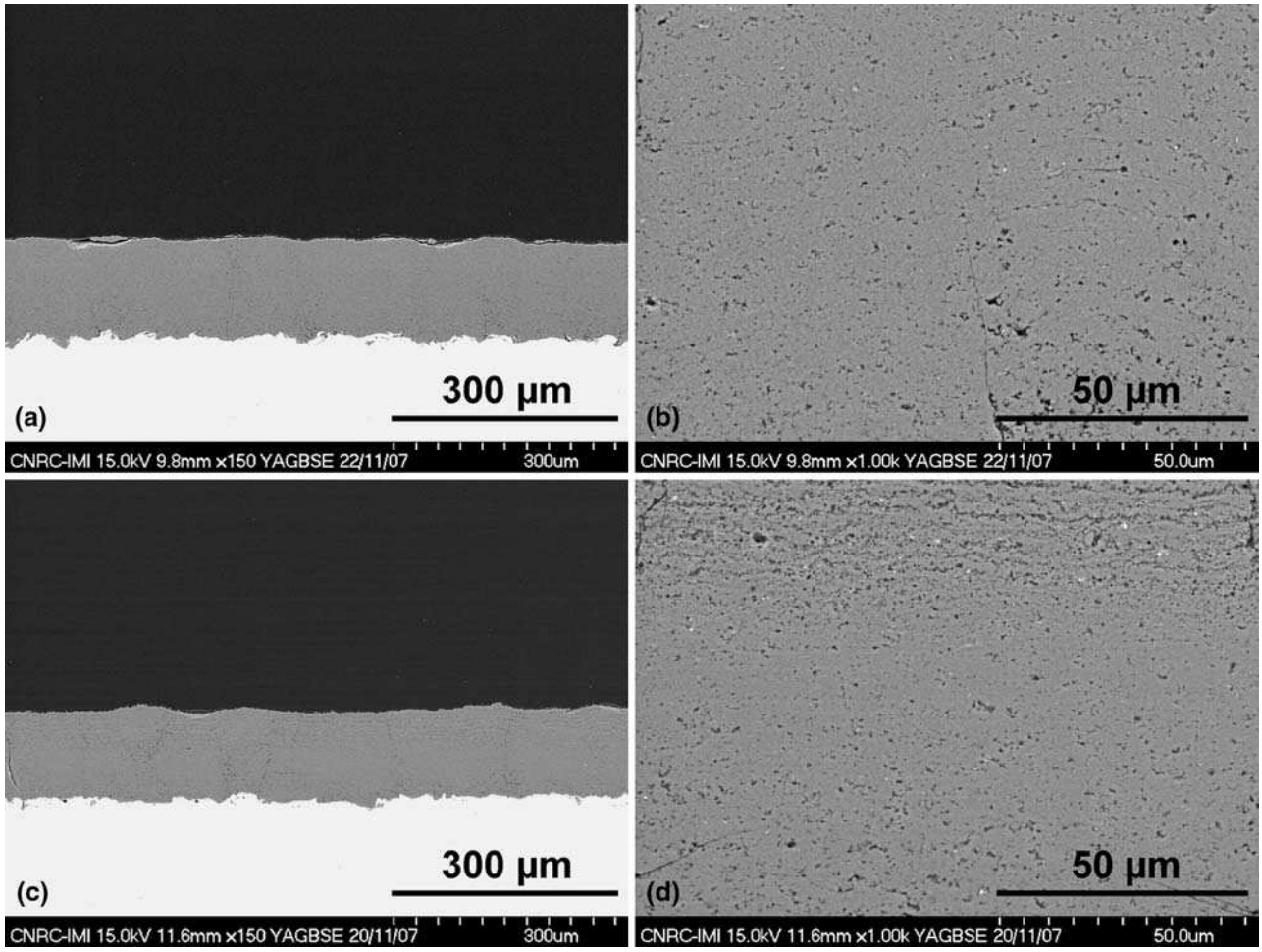

Fig. 14 Microstructures of DJ-2600 coating (a, b) H_2-450 (c, d) H_2-684 hot

are created from mostly molten particles, impacting at high velocity. A distinct difference from the coatings produced with propylene, in particular with respect to the crystalline content, cannot be discerned. It is possible that the background radiation emitted by the flame, which differs substantially between the DJ-2700 and the DJ-2600 jet, exaggerates the difference in particle temperature, as measured by the optical system. Furthermore, the information about the particle states at the short SD is subject to uncertainty since it is extrapolated from measurements further downstream. It cannot be excluded that at the short SD the particles are still in a process of heating, leading to the deposition of partially molten feedstock in some of the more crystalline DJ-2700 coatings.

Ultimately, the potential of HVOF over plasma spraying in terms of low flame temperature and the high velocity could not be fully exploited for suspension spraying of crystalline mullite coatings, since the particles experienced a dwell time long enough for complete melting in nearly all conditions investigated. However, allowing in situ crystallization by raising the substrate temperature during deposition can create fully crystalline coatings.

4. Conclusions

- The potential of HVOF with liquid suspension feed as a novel method to produce thin protective mullite coatings was explored. The lower flame temperature and high particle velocity, potentially limiting particle melting, make this technique a promising candidate.
- Mullite coatings with surface roughness $R_a < 3$ µm, with over 20% crystallinity and uniformly distributed and fine porosity below 2%, were produced with the DJ-2700 at high propylene fuel-to-oxygen ratios and at short standoff distance.
- Decreasing the flame temperature by reducing the fuel supply or changing to hydrogen fuel was not found to increase the crystalline content in the coatings. It was speculated that dwell time and not maximum flame temperature is the principal factor governing the degree of in-flight particle melting.
- Crystalline mullite coatings with porosities ≤2% and Vickers hardness ≥640 $Hv_{0.3}$ were produced with DJ-2700 and DJ-2600 by gradually increasing the surface temperature above 400 °C during deposition.

References

1. P. Rohan, K. Neufuss, J. Matějíček, J. Duvský, L. Prchlík, and C. Holzgartener, Thermal and Mechanical Properties of Cordierite, Mullite and Steatite Produced by Plasma Spraying, *Ceram. Int.*, 2004, **30**, p 597-603
2. F. Cipri, C. Bartuli, T. Valente, and F. Casdei, Electromagnetic and Mechanical Properties of Silica-Aluminosilcates Plasma Sprayed Composite Coatings, *Proceedings of the 2007 International Thermal Spray Conference*, *Global Coatings Solutions*, May 14-16 2007 (Beijing, China), ASM International, 2007, p 507-512
3. P. Ramaswamy, S. Seetharamy, K.B.R. Varma, and K.J. Rao, Thermal Shock Characteristics of Plasma Sprayed Mullite Coatings, *J. Therm. Spray Technol.*, 1998, **7**(4), p 497-504
4. K.N. Lee, R.A. Miller, and N.S. Jacoson, New Generation of Plasma-Sprayed Mullite Coatings on Silicon Carbide, *J. Am. Ceram. Soc.*, 1995, **78**(3), p 705-710
5. X.Q. Cao, R. Vassen, and D. Stoever, Ceramic Materials for Thermal Barrier Coatings, *J. Europ. Ceram. Soc.*, 2004, **24**, p 1-10
6. R. Vaβen and D. Stöver, Development of Thin and Gastight Ceramic Coatings by Atmospheric Plasma-Spraying, *Proceedings of the 2006 International Thermal Spray Conference, Thermal Spray: Building on 100 Years of Success*, May 15-18 2006 (Seattle, USA), ASM International, 2006
7. K.N. Lee, D.S. Fox, J.I. Eldridge, D. Zhu, R.D. Robinson, N.P. Bansal, and R.A. Miller, Upper Temperature Limit of Environmental Barrier Coatings Based on Mullite and BSAS, *J. Am. Ceram. Soc.*, 2003, **86**(8), p 1299-1306
8. P.H. McCluskey et al., ''Plasma Sprayed Mullite Coatings on Silicon Based Ceramic Materials,'' U.S. Patent 6,468,648 B1, 2002
9. I.T. Spitsberg et al., ''Method for Thermally Spraying Crack-Free Mullite Coatings on Ceramic Based Substrates,'' U.S. Patent 6,296,909 B1, 2001
10. R. Siegert et al., ''Production of Gastight, Crystalline Mullite Layer by Using a Thermal Spraying Method,'' PCT Patent Application WO2006034674, 2006
11. A. Killinger, M. Kuhn, and R. Gadow, High-Velocity Suspension Flame Spraying (HVSFS), a New Approach for Spraying Nanoparticles with Hypersonic Speed, *Surf. Coat. Technol.*, 2006, **201**, p 1922-1929
12. J. Oberste Berghaus, J.G. Legoux, C. Moreau, F. Tarasi, and T. Chraska, Mechanical and Thermal Transport Properties of Suspension Thermal-Sprayed Alumina-Zirconia Composite Coatings, *J. Therm. Spray Technol.*, 2008, **17**(1), p 91-104